CHAPTER 9

MIXING ACROSS DENSITY INTERFACES

In this chapter we will consider the processes of formation of mixed layers by externally driven turbulence, and entrainment of fluid across the interfaces bounding such layers. Mixing across a density interface has so far been treated only in the special context of double-diffusive convection (§8.3), but more general stirring mechanisms must now be discussed. The problems of interest here may be identified with cases (*d*) or (*e*) of fig. 4.19, in which stirring at one level is used to produce mixing across an interface located some distance below or above the source of turbulent energy.

Various laboratory experiments which have shed light on the mechanism of entrainment at a density interface will be described first. Mixing can be generated by mechanical stirring, or by the production of a mean turbulent flow in the surface layer, and both methods have been used. The observed structure of the surface layers of the ocean and atmosphere discussed in § 10.1 suggest that mixing in those regions is dominated by the boundary processes. The laboratory results can immediately be applied to these geophysical examples, and, with the addition of results from the earlier chapters on convection, they can be extended to take account of convective as well as mechanical mixing. It is assumed throughout this chapter that the mixing processes under consideration can be treated as one-dimensional in depth, implying that mixing is uniform (in the mean) over a large horizontal area, with no significant contribution from large scale lateral convection.

9.1. Laboratory experiments

9.1.1. *Stirring with oscillating grids*

A convenient way to study one-dimensional mechanical mixing in a stably stratified fluid is to use a vertically oscillated grid of solid

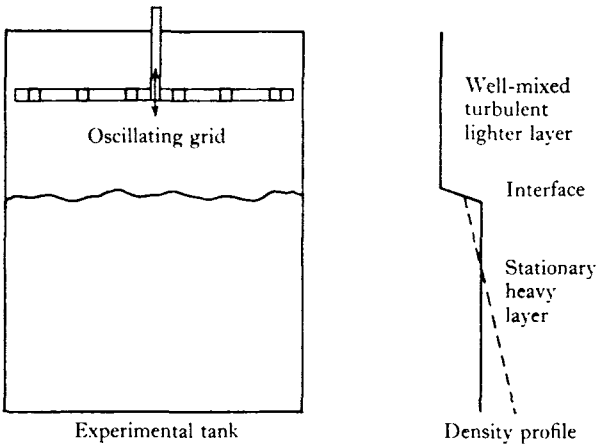

Fig. 9.1. Sketch of the experimental tank and stirring grid, and the density distribution produced by stirring.

bars (see fig. 9.1). Rouse and Dodu (1955) first applied this method in a two-layer experiment, and Cromwell (1960) stirred at the top of an initially stable density gradient. In both cases, a well-mixed layer is formed, bounded by a *sharp* interface which moves away from the stirrer as fluid is entrained across it from the quiescent fluid into the stirred layer. Thus the external stirring produces and maintains the well-mixed layer, and also sharpens the interface and causes the mixing across it. (This geometry corresponds to case (*e*) of fig. 4.19.)

The nature of the entrainment process is shown in the two photographs of fig. 9.2 pl. XXIII. When the stirred layer is dyed, one can see that large eddies of the imposed motion are thrusting into the unstirred fluid and trapping some of it between them, whereas smaller scale motions are rapidly damped. (In a uniform density gradient the larger eddies would be damped first – refer to the discussion of the 'buoyancy subrange' in § 5.2.2, and the experiments of Grigg and Stewart (1963). The new point here is that the eddies which dominate the entrainment process are larger than the thickness of the interface and are outside it, so they are substantially unaffected by the interfacial density gradients.) On the other hand, when the unstirred fluid is dyed (fig. 9.2*b*) thin sheets of entrained fluid are at first visible, before being rapidly mixed through the whole

of the stirred layer. There is too little evidence to judge yet whether this entrainment process is a slightly modified version of that occurring at the edge of a turbulent plume or jet (§6.1.1) or whether the density step introduces an essentially different mechanism.

There have been few detailed measurements of interfacial structure in these experiments, though visual observations give some important clues. The instantaneous thickness of the interface decreases as the stirring rate is increased, but this thickness depends only very weakly on the property being transferred. Thus the transfer cannot be described as a simple balance between molecular diffusion and large scale stirring, and indeed it can be shown that under typical laboratory conditions an interface sharp enough to transfer even the measured heat fluxes by pure diffusion will be unstable to the shear instability mechanism described in §4.1. The mixing takes place largely through a process which looks like the intermittent breaking of steep forced internal waves, which tends to thicken the interface, followed by the sweeping away of this fluid by the stirring in the layers, which sharpens the interface again.

Most quantitative measurements of mixing rates have been interpreted using arbitrary overall measures of length and velocity scales, derived from the geometry and stirring frequency. Thompson (1969) has gone a step further, and has shown how one can relate the entrainment rates to the properties of the turbulence. Using a hot-film technique he measured an integral lengthscale l_1, and the r.m.s. value u_1 of the horizontal component of the turbulent velocity, as functions of the distance z from the grid in the same apparatus which had been used earlier (Turner 1968*b*) to measure entrainment rates. Over a comparable range of conditions, and using the same grid of square bars, Thompson showed that u_1 remains proportional to the stirring frequency while the turbulence decays rapidly with increasing z, and that l_1 increases linearly with z. (With other geometries of stirring grid, however, the relations were not so simple, and this can lead to ambiguities in the interpretation of mixing rates in other experiments. See §9.1.3.)

Thus one can now be confident that the entrainment rates measured in Turner's experiments have been related to scales which are not arbitrary, but are characteristic of the fluid motion near the interface. By a similar argument to that used in §6.2.1 for a

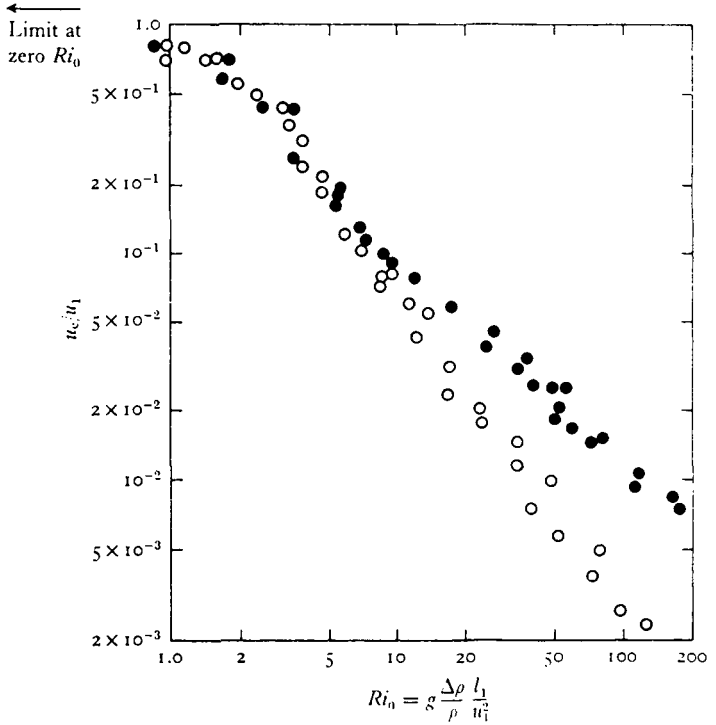

Fig. 9.3. A comparison between entrainment velocities produced by a stirring grid, across density interfaces formed with • temperature differences and ○ salinity differences. The dimensionless mixing rates obtained by Turner (1968*b*) are plotted logarithmically against an overall Richardson number, using the length and velocity scales l_1 and u_1 suggested by Thompson (1969). These are genuine flow parameters, though their numerical values are subject to revision.

turbulent gravity current, we can suppose initially that the mixing process represents a balance between buoyancy and inertia forces alone. The entrainment velocity u_e will then be a function of l_1, u_1 and the density difference $\Delta\rho$ between the layers, which can be expressed as

$$u_e/u_1 = f(Ri_0), \tag{9.1.1}$$

where

$$Ri_0 = g\Delta\rho l_1/\rho u_1^2$$

is another overall Richardson number. The experimental results (with stirring in one layer) shown in fig. 9.3 support the choice of Ri_0 as the major governing parameter. As $Ri_0 \to 0$ and the buoyancy effects become negligible, u_e again approaches a constant fraction of

u_1, and u_e falls as Ri_0 increases. Notice, however, that the functional forms shown on fig. 9.3 for the rates of mixing with temperature or salinity differences across the interface are *different*, so there is also a molecular effect, which will be discussed further in §9.1.3.

When *both* layers are stirred in similar experiments, it is found that the mixing rate (in one direction) is not substantially changed (though now, of course, an indirect measure of u_e must be used, based on the rate of change of properties in the layers). This implies that not only is the turbulence very strongly damped at an interface, but the events which cause the removal of fluid are so rare that the two sides can be regarded as statistically independent. When the stirring is applied at the same rate in the two layers, the interface remains sharp and central. If stirring is unsymmetrical, the interface moves away from the region of more vigorous stirring until the entrainment rates on the two sides balance. Superficially, the two-layer system with stirring on both sides of an interface has much in common with the double-diffusive interfaces treated in §8.3, since in both cases the interface is kept sharp by turbulence in the layers on each side. The latter are complicated, however, by the double boundary layer structure and by the fact that the stirring is through convection driven by the interfacial flux; no theoretical framework which can include both of these has yet been suggested.

9.1.2. *Mixing driven by a surface stress*

Grid stirring is experimentally convenient, and it will also be relevant for modelling natural processes in which turbulent energy is put in on a scale much smaller than the layer depth (for example, by the breaking of waves at the sea surface; see §9.2.1). It does impose a rather special structure characteristic of the grid, however, and various experimenters have suggested other techniques for producing a turbulence structure which is related to the geometry of the flow alone. As we have seen earlier, turbulence is often produced by a boundary stress, either at the bottom (as in §6.2 – see fig. 6.9), or by the action of a wind on the surface of the sea (§5.3.2), and in both these cases there will be a mean flow as well as turbulence.

Kato and Phillips (1969) have reported a laboratory experiment designed to model this latter process directly. To avoid end effects

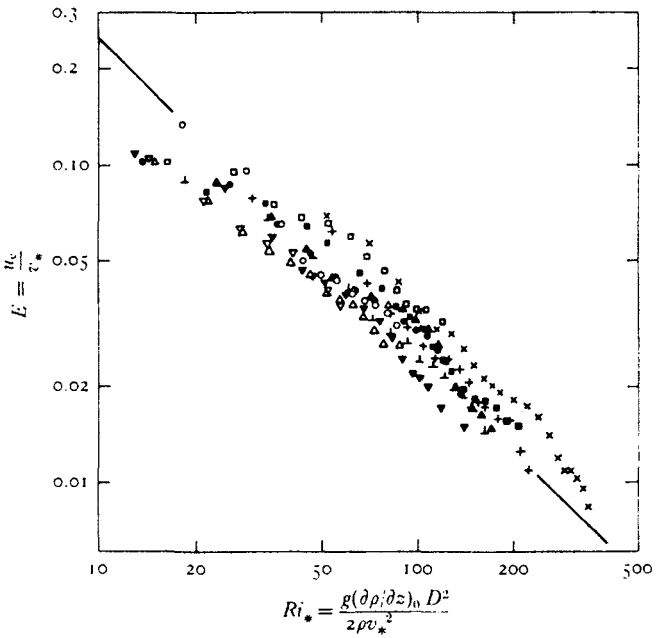

Fig. 9.4. Entrainment rates measured by Kato and Phillips (1969) in a turbulent stratified flow produced by a surface stress. The overall Richardson number is defined using the friction velocity and the depth of the mixed layer, and different symbols are used for experimental runs with various initial density gradients and surface stresses.

they used an annular tank containing salt solution with a linear density gradient, and applied a controlled constant stress τ at the top by rotating a plastic screen immersed just below the surface. During the first few seconds of motion they observed a regular train of waves, aligned across the flow, arising from a shear instability of the kind discussed in §4.1. These quickly broke down, and a turbulent layer formed, bounded below by a sharp interface which advanced at a decreasing rate and across which the density difference was increasing with time. (Compare with the layer growing by convection, fig. 8.8.)

Their measurements of the layer depth D as a function of time, together with the known initial gradient and the imposed stress, can be plotted non-dimensionally in the form shown in fig. 9.4. The dimensional argument which led to (9.1.1) now suggests that

$$E = u_e/v_* = f(Ri_*), \qquad (9.1.2)$$

where the friction velocity in the water (defined by $\tau = \rho_0 v_*^2$) is used as the velocity scale and

$$Ri_* = \frac{g\Delta\rho D}{\rho_0 v_*^2} = \frac{g(\partial\rho/\partial z)_0 D^2}{2\rho_0 v_*^2}. \tag{9.1.3}$$

The observations are not inconsistent with this prediction, but the scatter is considerable and the range of E rather small, so there is some uncertainty in fitting a curve to these points.

A particular form of this function is suggested by a rather more explicit dimensional argument than the one used above, which also has an attractive physical interpretation. If $\Delta\rho$ and u_e are supposed to be separately unimportant, and to occur only as the product $(g\Delta\rho/\rho)u_e$ (i.e. the buoyancy flux across the interface) then dimensional reasoning gives

$$\left.\begin{aligned} g\Delta\rho u_e D &\propto \rho v_*^3, \\ \text{or rearranging,} \qquad E &\propto Ri_*^{-1}. \end{aligned}\right\} \tag{9.1.4}$$

The first form of this relation is equivalent to the statement that the rate of change of potential energy V, say, of the well-mixed layer is proportional to the rate of working of the surface stress. It also implies, incidentally, that the rate of change of density of the layer is independent of the density difference, for a fixed rate of working.

The numerical constant obtained by fitting this form to Kato and Phillips' (1969) experiments over the range $30 < Ri_* < 300$ (see fig. 9.4) implies that

$$\frac{u_e}{v_*} = 2.5 Ri_*^{-1} = 2.5\frac{\rho_0 v_*^2}{g\Delta\rho D} \tag{9.1.5}$$

and also that

$$\frac{dV}{dt} = \tfrac{1}{2} g\Delta\rho D u_e = 1.25\rho v_*^3. \tag{9.1.6}$$

J. B. Hinwood (personal communication) has found that these (and various other experimental results) fit this simple assumption rather better if the change in potential energy of the whole profile, including the detailed structure of the interface, is used instead of that based on the layer alone (with the interface regarded as a simple step).

Qualitative observations in Kato and Phillips' experiment at much later times (and greater mixed layer depths) showed that

viscosity can eventually become important. The rate of increase of depth, and the amplitude of wave motions at the interface, became very small, but a drift velocity was observed below the interface. A layer of increasing depth was set into motion by the viscous stress across it, and at this stage viscosity will also be damping the waves (cf. §2.4.2) and affecting the entrainment rate. The possibility that some momentum is extracted in the form of waves propagating into the stable gradient will be considered in §9.2.

A more elaborate experiment along the same lines has been described by Moore and Long (1971). They produced a steady turbulent stratified flow in a cyclic tank by injecting and withdrawing fluid through the floor and ceiling. As is to be expected in a flow which is driven at the boundaries, two homogeneous layers formed, separated by a thin interface. Experiments with one or both layers flowing were interpreted in a similar overall way to that already described. Detailed profile measurements were also made, and these indicate that the gradient Richardson number through the interface has a value of order one.

9.1.3. *The influence of molecular processes*

An explicit dependence of mixing rate on Reynolds number was proposed by Rouse and Dodu (1955) on the basis of their grid stirring experiments. The more recent measurements suggest, however, that this interpretation may be inappropriate, and a consequence of their use of the grid frequency as a measure of the velocity near the interface, under conditions where this assumption was not justified. In other words, their results could be an indication of a viscous effect occurring near the generating grid, rather than during the decay process or near the interface. Viscosity can certainly affect motions across very stable interfaces at low Reynolds number, but there is a substantial range of conditions where it can be ignored even in the laboratory.

Whatever view one takes about the importance of viscosity, it cannot be used to explain the results shown in fig. 9.3. Since these experiments were conducted with essentially constant viscosity, and the same range of density differences and stirring rates, the large differences in u_e using salt and heat can only be explained by

invoking the molecular diffusivity. A second dimensionless parameter must enter the problem; this can be taken as a Péclet number, say $Pe = u_1 l_1/\kappa$, so (9.1.1) is replaced by

$$u_e/u_1 = f_1(Ri_0, Pe). \tag{9.1.7}$$

In these experiments u_1 and l_1 were varied little, so the major change of Pe was due to the change in κ. Effectively Pe had two different constant values, one for salt and another for heat, and the experimental curves are just two sections of the surface $f_1(Ri_0, Pe)$. These tend to the same form at low Ri_0 (where neither buoyancy nor diffusion is important) but diverge at larger Ri_0, becoming approximately $u_e/u_1 \propto Ri_0^{-1}$ (heat) and $u_e/u_1 \propto Ri_0^{-\frac{3}{2}}$ (salt).

The apparent correspondence between the results with temperature differences and the 'energy' argument (implied by (9.1.4)) led Turner (1968*b*) to suppose that the Ri_0^{-1} law is in some way fundamental, and that the salt flux is reduced relative to this because of a slower incorporation of an entrained element into its surroundings by diffusion. More recent evidence supports the contrary view. C. G. H. Rooth (personal communication) has used a wider range of stirring rates, in experiments with temperature differences across an interface, to show that the basic rate of entrainment in the buoyancy controlled turbulent regime at large Pe (u_1 large) is close to

$$u_e/u_1 \propto Ri_0^{-\frac{3}{2}}$$

in the range studied. As Pe is reduced, the curves break away from the $Ri_0^{-\frac{3}{2}}$ line at successively lower values of Ri_0, rising above it with decreased slope as molecular diffusion increases the transfer rate. (The tendency can also be detected in fig. 9.3.) Baines (1975) has investigated the mixing across an interface caused by a turbulent plume or jet directed normal to it, and his results also support the $Ri_0^{-\frac{3}{2}}$ form.

A mechanistic explanation of the $Ri_0^{-\frac{3}{2}}$ mixing law in terms of inertial and buoyancy forces alone has recently been proposed by Linden (1971*b*). He has projected vortex rings against an interface and has observed the characteristics of the depression produced by the ring over a range of approach velocities and density differences. His experiments suggest that the important transport mechanism is the storage of energy in the deflected interface, followed by ejection

of a jet up the centre on a timescale which is determined by the density difference and the scale of the eddies. The increased distortion of the interface at low Richardson numbers is the important factor which had previously been neglected.

At very large values of Ri_0, all the mixing curves flatten out and ultimately become independent of Ri_0. This last limit was studied by Fortescue and Pearson (1967) in the context of gas absorption into a water surface. They showed experimentally that u_e/u_1 is proportional to $Pe^{-\frac{1}{2}}$, and explained this using a theory based on molecular diffusion into the large eddies of turbulence in the water. Their arguments also seem appropriate for a very stable liquid–liquid interface.

9.1.4. *Comparison of various methods of stirring*

Several different mechanisms for the production of the turbulence which is responsible for mixing at density interfaces have now been discussed – surface jets and bottom currents in chapter 6, oscillating grids and a surface stress in this chapter – and it seems useful now to try to compare them. Absolute comparisons are uncertain because of the variety of length and velocity scales used, and it is not possible to judge yet, for example, whether a given level of turbulence is more effective in a mean shear flow than it is in a stirred box. Eventually one must decide how to relate the mean, turbulent and friction velocities in different geometries, but provided all the scales used are genuine flow parameters, much can be learned just from the shape of the curves. On a logarithmic plot of u_e/u_1 against Ri_0, the choice of l_1 and u_1 affects the magnitudes but not the slope.

In fig. 9.5 are plotted all the available results. The scales are appropriate for the grid stirring experiments transferred from fig. 9.3 (full lines, labelled I) but they must be regarded as arbitrary for the other data. The dotted outline II shows the range of entrainment rates obtained by Kato and Phillips and previously plotted in fig. 9.4; this has been placed at the value of Ri_0 where the curves are flattening out on the left. The upper dashed line III is taken from the experiments of Ellison and Turner (previously plotted as the full line in fig. 6.8), which has been fitted so that u_e/u_1 is the same as $Ri_0 \to 0$ and the curves match at small Ri_0. (Note that this differs

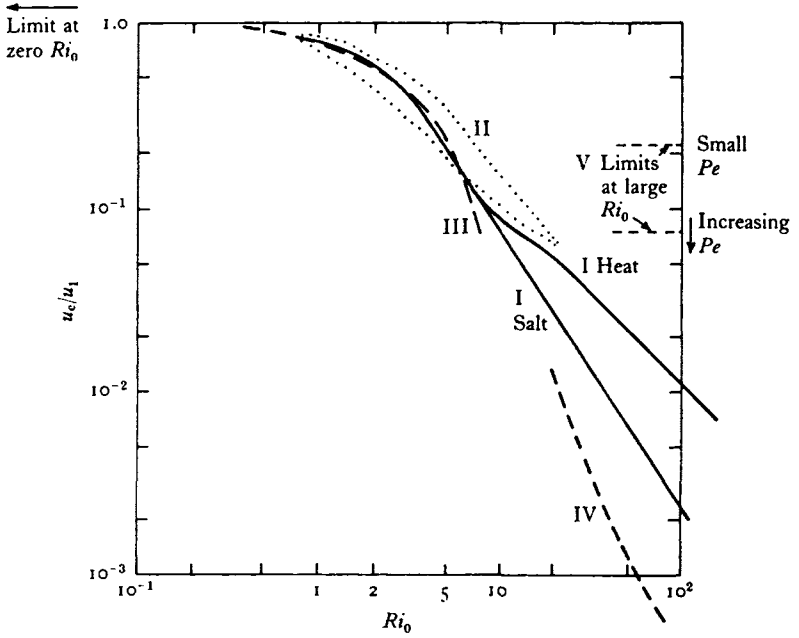

Fig. 9.5. Comparison of entrainment rates as a function of overall Richardson number for various methods of production of the turbulence. The scales are transferred from the earlier plot of I, but are arbitrary for the other curves. I Grid stirring (fig. 9.3). II Surface stress (fig. 9.4). III Bottom current on steep slope (fig. 6.8). IV Bottom current on low slope (fig. 6.8). V Limits at large Ri_0.

from all the other experiments shown, in that *interfacial* stresses dominate in the production of turbulence.) The lower dashed line IV (due to Lofquist, and also shown in fig. 6.8) is scaled in exactly the same way as III. The limits for large Ri_0 and various values of Pe are shown as the dotted lines on the right, marked V.

When compared in this way, the measurements suggest the following generalizations. In the limit of high Re and high Pe, u_e/u_1 is a function of Ri_0 alone, approaching a constant value as $Ri_0 \to 0$ and having the approximate form $Ri_0^{-\frac{3}{2}}$ at intermediate Ri_0. As Pe decreases, the mixing rate is increased and the curves break away from the high Pe limit at successively smaller values of Ri_0; at large Ri_0, u_e/u_1 approaches a constant value proportional to $Pe^{-\frac{1}{2}}$. The curves III and IV suggest that a similar statement can be made about the effect of Reynolds number. When Re is reduced the

mixing rate is also reduced, the break from the high Re curve coming at lower values of Ri_0 the smaller the scale of the experiments. The mechanism whereby viscosity affects the mixing, whether by increasing the rate of decay in the turbulent layer or (more probably) by damping the interfacial waves, awaits a detailed study.

9.2. Geophysical applications

9.2.1. *The wind-mixed surface layer*

The above results will now be applied to the problems of mixing across oceanic thermoclines and atmospheric inversions. We first consider the case where the stirring is entirely mechanical, and driven by the wind stress at the surface of the sea. The effects of geometry and a stabilizing buoyancy flux must also be taken into account here, so that cases (*e*) and (*f*) of fig. 4.19 become relevant, as well as (*d*). A later step will be to add convective stirring, using some of the results introduced in chapters 7 and 8.

Let us suppose that the mixing at the bottom of the surface layer can be described by (9.1.4), derived above using dimensional reasoning (but also shown to be equivalent to an energy argument). This is a convenient (but not essential) assumption which simplifies the subsequent analysis while retaining all the important qualitative features. If the upper ocean can be described as a two-layer system, with a surface layer of constant total buoyancy and depth D lying above a deep column of uniform density, the rate of change of potential energy V as the layer deepens due to mixing across the interface is

$$\frac{\mathrm{d}V}{\mathrm{d}t} = \tfrac{1}{2}(gD\Delta\rho)\frac{\mathrm{d}D}{\mathrm{d}t} = \tfrac{1}{2}bu_e. \qquad (9.2.1)$$

Thus with a fixed rate of input of mechanical energy and no buoyancy flux across the sea surface, the interface will descend at a constant rate, which is inversely proportional to the total buoyancy b. (Other mixing laws, with given v_*, will still give a constant rate of descent depending on b alone, though the functional form will be different.)

With an arbitrary initial density distribution in the water column $\rho(z)$, a relation of the form (9.1.4) (or more generally, (9.1.2)) will

still hold, and this can be integrated to give D as a function of t using

$$\bar{\rho} = \frac{1}{D}\int_0^D \rho(z)\,\mathrm{d}z \tag{9.2.2}$$

and

$$\Delta\rho = \rho(D) - \bar{\rho}$$

to evaluate the density jump at each stage. For example, with a linear density gradient the energy argument gives

$$D(t) = v_*\left(\frac{15t}{N_0^2}\right)^{\frac{1}{3}}, \tag{9.2.3}$$

N_0 being the initial buoyancy frequency. Though the stress in this case is applied by a wind blowing over the surface, v_* is still the friction velocity in the water (i.e. defined using the stress and the density of water).

The numerical factor in (9.2.3) has been taken from (9.1.6), but it is most unlikely that the laboratory experiments in question adequately reproduce all the relevant processes. It is observed, for example, that the motion of an oceanic mixed layer can become organized into long rolls aligned downwind (the Langmuir cells), which will result in a stronger stirring on the scale of the whole layer depth. The presence of surface waves (and their suppression in the laboratory) could also have a significant effect on the energy transfer process. The total rate of working of the wind on the water is much larger than $v_*\tau$ (it is more nearly $c\tau$, where c is the phase velocity of the waves) and even if only a small fraction of this energy were eventually used for mixing, it could increase the estimate based on the stress alone. The analysis of some direct observations of the transient deepening of shallow surface layers (Turner 1969*b*) does suggest that the factor in (9.2.3) might be as much as twice as great.

For very deep wind mixed layers, v_* is not likely to remain the relevant velocity parameter. Turbulent energy put in through the breaking of waves near the surface will have a smaller scale than the layer thickness (cf. fig. 4.19*e*). It will decay with depth and be less effective for mixing, as does the grid-generated turbulence discussed in §9.1.1. More will be said about deep layers in the next section, in the context of convectively driven mixing.

9.2.2. *Seasonal changes of a thermocline*

An extension of these arguments can be applied to the description of the longer term behaviour of the thermocline, but it is essential then to take into account the surface heating and cooling as well. During periods when the surface is being heated, and both the heating rate and the rate of input of mechanical energy are constant, the depth can remain fixed at a value D_1. This is the result of a delicate balance between two opposing effects (since surface heating tends to make the layer shallower and the stirring to deepen it), and is given by

$$D_1 = av_*^3/(\overline{g'w'}) = av_*^3/B, \tag{9.2.4}$$

where B is the buoyancy flux (which in general should include the effects of salinity variations cf. (5.3.6)). This form was first suggested by Kitaigorodskii (1960) using dimensional reasoning similar to that which leads to the Monin–Obukov length L (§ 5.1.2). It is based on the same concepts as (9.1.4), the only difference being the source of the buoyancy flux. Equation (9.2.4) implies that the kinetic energy input, proportional to v_*^3, is being used to change the density of the upper layer by mixing light fluid from the surface through the whole depth D_1 (case (*f*) of fig. 4.19). The mean value of $a = 2$ which Kitaigorodskii obtained using selected ocean data agrees approximately with Kato and Phillips' measurements, but the choice of a numerical value here and in the extension of this model described below is subject to all the uncertainties mentioned earlier.

When the heating rate is increasing, the thermocline will rise and the upper layer will warm, leaving previously affected layers of fluid below it; as shown by (9.2.4) a given stirring energy can now mix a larger buoyancy input only to a shallower depth. When the rate of heating is decreasing (but still positive) the upper layer will continue to warm, but will begin to deepen slowly as fluid from the gradient set up earlier is entrained across the sharp interface below it. Finally, when the surface is being cooled, there will be a more rapid cooling and deepening of the upper layer. During this stage another assumption must be made, regarding the proportion of the convective energy which is available for entrainment (cf. §§7.3.4, 8.2.1); more will be said about this in the following section.

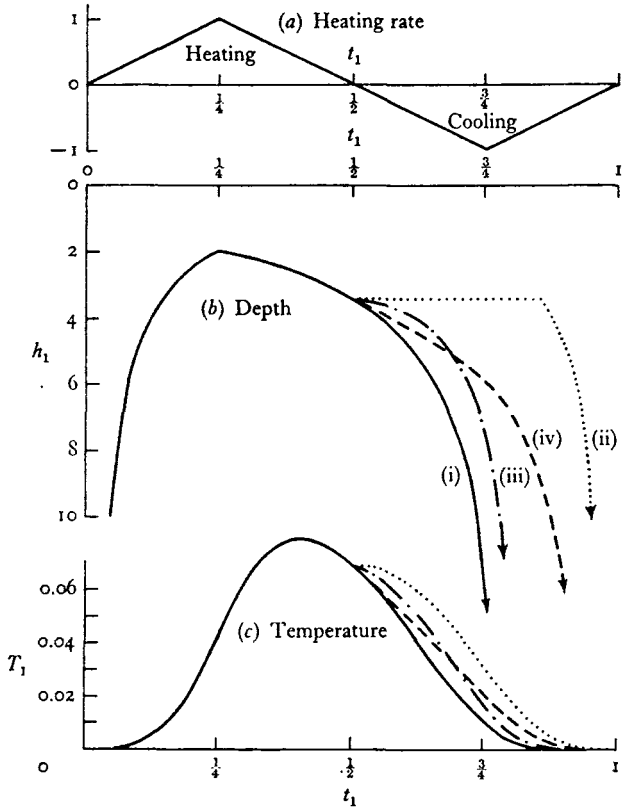

Fig. 9.6. Non-dimensional plots of the mixed layer depth h_1 and surface temperature T_1 as functions of time t_1, calculated for a saw-tooth heating and cooling function and a fixed rate of mechanical stirring. Curves (i) are based on the original energy-conserving assumption of Kraus and Turner (1967); (ii) assume no penetration at all during the cooling phase; (iii) take account of the entrainment due to convection alone, and (iv) include only the entrainment produced by the mechanical stirring. (After Kraus and Turner 1967.)

These ideas have been applied to situations where the surface buoyancy flux varies cyclically, as it does during the course of a year. A completely steady state (with the heat input at the surface exactly balancing the cooling over the year) is unlikely in the ocean without some advection, but this is nevertheless a useful case to study. Kraus and Turner (1967) treated an idealized 'saw tooth' heating and cooling cycle, with the rate of mechanical working

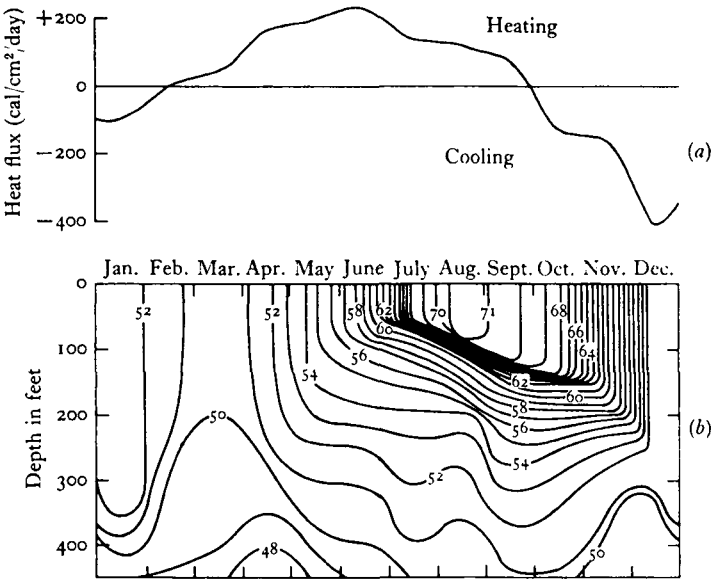

Fig. 9.7. (*a*) A typical annual heating and cooling cycle observed in an area of small advection (the subarctic Pacific) compared with (*b*) the variation of temperature with depth in the same region. Contours are marked in °F. (See Tully and Giovando 1963 for a more detailed discussion of this structure.)

assumed fixed. All the features described above can be picked out in fig. 9.6, where the full lines show the annual variations of layer depth and surface temperature calculated with these boundary conditions, using the principles outlined in the next paragraph. A laboratory experiment which modelled the buoyancy fluxes using fresh and salt water also supported the main conclusions of this theory.

The whole of the deepening process in this model can be described using the time-integrated buoyancy and mechanical energy equations

$$\rho_s D - \int_0^D \rho(z)\,\mathrm{d}z = \int_{t_0}^{t} \frac{\rho_0 B}{g}\,\mathrm{d}t, \tag{9.2.5}$$

$$\tfrac{1}{2}\rho_s D^2 - \int_0^D \rho(z)\,z\,\mathrm{d}z = \int_{t_0}^{t} \frac{G}{g}\,\mathrm{d}t. \tag{9.2.6}$$

These simply express the assumptions that in passing from an arbitrary density distribution $\rho(z)$ to a step of depth D and density ρ_s, the changes in buoyancy and potential energy are equal to the

integrated inputs of buoyancy B and effective mechanical energy G during the deepening process. Equation (9.2.6) implies that there is no dissipation, a point which will be taken up again in the following section. Scaling the equations with $G/\rho = G_*$, a characteristic value of B (say $B_{\max}$) and the period P of the heating cycle (a year in the case treated) gives the functional dependence on the external parameters:

$$g\alpha T_{\max} = c_1 B_{\max}{}^2 P/G_* \tag{9.2.7}$$

and

$$h_{\min} = c_2 G_*/B_{\max} \tag{9.2.8}$$

(cf. (9.2.4)). The multiplying constants c_1 and c_2 depend on the exact shape of the heating function; for example, with this scaling, c_1 is 0.12 for a sinusoidal heating function compared with 0.08 for the saw-tooth form.

The predicted behaviour should be compared with the measurements shown in fig. 9.7, which were made in an area where advection is small and the one-dimensional model should be appropriate. Most of the qualitative features are well reproduced, especially the phase relationship between the time of maximum heating and minimum depth (which occur together), and maximum surface temperature (which comes later). The physical assumptions underlying this model are also well supported by the more detailed observations summarized by Tully and Giovando (1963), who have explained them qualitatively in very similar terms. One feature is not predicted by the model described above, namely, the change in depth with time of the isotherms below the well-mixed layer. This implies continuing mixing in this deeper region, which must be due to energy propagating beyond the interface, in the form of internal gravity waves. Direct evidence for the process is also to be found in the observations, and it will be discussed further in § 10.3.3.

Also drawn on fig. 9.6 are the results of varying the energy conservation assumption in various ways during the cooling cycle only. The dotted lines (ii) show what happens when there is *no* penetration of the interface, driven either mechanically or convectively; the surface layer just cools without deepening until the density step is removed, then it deepens in a way which can be calculated using the heat balance alone (see §9.2.3). (This last assumption is supported by the work of Anati (1971), who showed

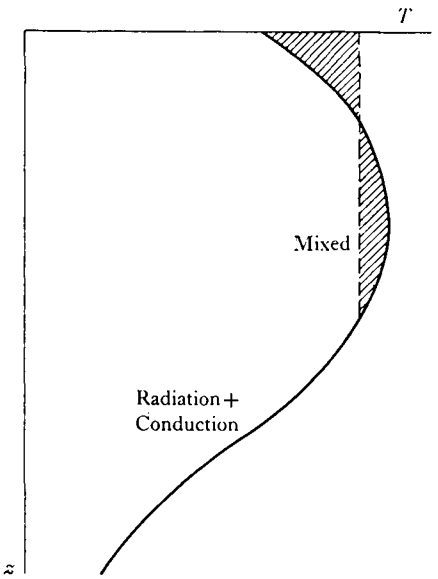

Fig. 9.8. Illustrating the formation of a mixed layer by the absorption of radiant heat in the interior combined with cooling due to evaporation at the surface. A heat balance alone has been assumed here, with no extra entrainment at the bottom of the mixed layer.

that the growth of a very deep well-mixed layer in the Mediterranean is described well using a non-penetrative model based on the density distribution and the net buoyancy flux. In that area in winter, vigorous mixing is produced by rapid surface cooling resulting from strong winds.) The dashed lines on fig. 9.6 show the penetrative effects of the two components, supposing that they can be considered separately. It is clear that whatever assumption is used, surface cooling and not mechanical mixing eventually has a dominant influence on the deepening process, though the time at which the deepening occurs does depend on the other factors.

In some cases it is essential to allow for stirring due to the absorption of radiated heat in the interior. Kraus and Rooth (1961) showed that the depth of a convective layer depends largely on the balance between the interior heating and the surface cooling due to evaporation; this effect too can be combined with mechanical stirring. Again one has to make an assumption about the fraction of the kinetic energy generated by the convective overturning which is

used in entraining heavier fluid from below. The evidence in the laboratory and in lakes (Dake and Harleman 1966) and in the ocean (Defant 1961, vol. 1, ch. 3) suggests that this fraction is small. Thus the mixed layer depths in the absence of wind can be calculated using the heat balance alone, and replacing the hydrostatically unstable parts of the temperature profiles (which would otherwise result from the combination of radiation and conduction) by a well mixed layer with the same heat content and no temperature step below. (See fig. 9.8.) A model which develops this same idea for the diurnal temperature cycle has recently been proposed by Foster (1971*a*).

9.2.3. *Mixing at an atmospheric inversion*

Theories of the development of the surface layer in the atmosphere have emphasized the stirring due to convection, though shear-driven turbulence can be important in this case too. The effect of a destabilizing buoyancy flux through a bounding surface is appropriately discussed in more detail in this context, and we can now add to the ideas about penetrative convection which were introduced in earlier chapters.

The results discussed towards the end of the previous section are also very relevant here. The rate of growth of a convecting layer into a region of stable temperature gradient will depend not only on the heat flux, but also on the rate of entrainment across the edge of the layer. The laboratory experiments of Deardorff, Willis and Lilly (1969) described in §7.3.4, and the corresponding experiments using a salinity gradient rather than a temperature gradient (§8.2.1), suggested that this effect is small. If viscous damping were significant in these experiments, then they might underestimate the importance of entrainment on the atmospheric scale, but the oceanic examples already given suggest that one will not go far wrong if the extra entrainment is ignored, and the convective layer depth is calculated using heat balance alone.

The opposite view was taken by Ball (1960), who calculated the variations in the height of an inversion on the assumption that *all* the energy produced by convection is available to entrain fluid across the top of the well-mixed layer. Though the energy-conserving case is still a useful limit to consider, this assumption is

certainly unrealistic in its extreme form, and not consistent with what is now known about the convection and mixing processes. If convection occurs in the form of 'thermals', for instance, it was shown at the end of §6.3.1 that only a small fraction of the work done by buoyancy appears as kinetic energy of mean motion, and similar results hold for other convection elements. Thus even if all of this energy on the larger scales which are most effective for entrainment were used for this purpose (and this is by no means certain) there would already be a substantial reduction in mixing rate.

When the individual convection elements are taken into account, we should also bear in mind the 'filling box' mechanism described in §7.3.3. This can produce a weak stable stratification even in conditions of strong convection, an effect which has been observed in the atmosphere by Warner and Telford (1967). (The experiments of Baines (1975) which were mentioned in §9.1.3 include both this effect and the entrainment by a plume at the interface.)

It is again useful to write down some special results, derived from (9.2.5) and (9.2.6) for the case of a linear initial density gradient specified by N_0^2, with various buoyancy fluxes and the two extreme mixing assumptions. The results given in §8.2.1 corresponding to a constant flux B_0 can be rewritten for the present purpose as

$$D = (6B_0)^{\frac{1}{2}} N_0^{-1} t^{\frac{1}{2}}, \quad g\frac{\rho_0 - \rho_s}{\rho_0} = (\tfrac{8}{3}B_0)^{\frac{1}{2}} N_0 t^{\frac{1}{2}}, \tag{9.2.9}$$

where ρ_0 is the initial density at the ground and ρ_s that in the well-mixed layer. The constants given are upper limits corresponding to the assumption of no energy loss; as explained previously, they are reduced, though the power law dependence remains the same, when the heat balance equation alone is used and there is no penetration. Note that this change in depth with constant heating is more rapid than it is with constant mechanical stirring (the time dependence is $t^{\frac{1}{2}}$ instead of the $t^{\frac{1}{3}}$ predicted by (9.2.3)). For a linear density gradient and a linearly increasing flux $B_0 = Ct$ the corresponding solutions are also linear in time, the assumption of no energy loss giving

$$D = (3C)^{\frac{1}{2}} N_0^{-1} t, \quad g\frac{\rho_0 - \rho_s}{\rho_0} = \left(\frac{4C}{3}\right)^{\frac{1}{2}} N_0 t. \tag{9.2.10}$$

The multiplying constants with no penetration are both $C^{\frac{1}{2}}$.

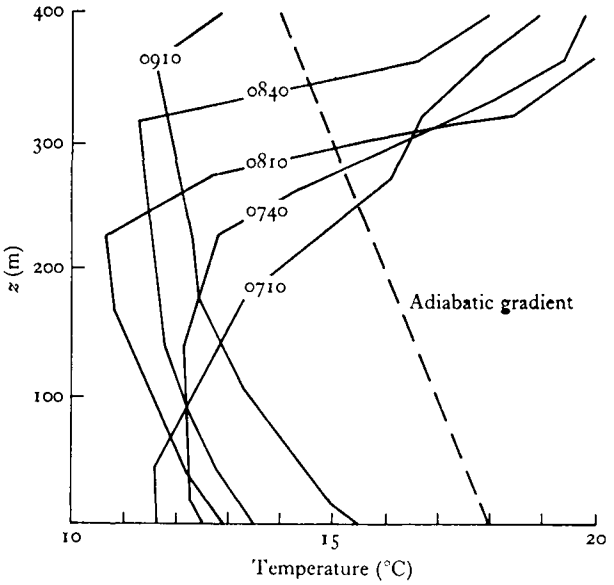

Fig. 9.9. Temperature profiles recorded by Izumi (1964) in the lower atmosphere as a mixed layer grew during the course of a morning. (The numbers on the curves are local times.)

Whatever the form of heating, there is a clear qualitative difference between the predictions in the two limiting cases. With penetration, the temperature at a given level will first fall abruptly as the step produced by entrainment passes a given level, and then gradually rise again. If there is no penetration, and just a change in gradient, the temperature at a fixed height can never decrease. Direct evidence for such a decrease in temperature (and therefore for extra mixing at the top of an atmospheric surface layer) was obtained by Izumi (1964), who followed the growth of a layer to about 400 m as the heat flux increased during two hours in the early morning (see fig. 9.9). Using these measurements, which were made when there was a strong wind, it is not easy to separate convective and mechanical energy inputs, however. It would be worth seeking examples of the convective growth of a well-mixed layer under conditions of no wind, to compare with those described in §9.2.1 for which the mechanical effect alone was believed to be relevant. There also seem to be some discrepancies between results obtained

in the atmosphere and ocean, which may result from different mechanisms and scales of turbulent energy generation, but which can only be clarified by further observations of carefully documented natural phenomena.

The same kind of description can be extended to moist convection in the atmosphere, and to much larger scales. Riehl *et al.* (1951), for example, found evidence for entrainment through the trade wind inversion, the mixing elements in that case being cumulus clouds. The inversion acts as a lid for humidity, since the transport of properties by the entrainment process is always downwards into the turbulent layer; the consequent tendency of the inversion to rise is counteracted by large scale subsidence. Lilly (1968) added radiative cooling at the top of a convective layer to the heating below, and studied theoretically both the dry and the moist cases. He, too, used the two extreme assumptions about the conversion of energy, but a detailed discussion of his results would bring in the new effect of heat radiation, which it is not appropriate to pursue here. Note, however, that if losses of heat at the top are allowed, the existence of a step is *not* an indication that penetrative mixing is occurring.

We have emphasized the convectively unstable atmospheric surface layers, but mention should also be made here of some results obtained in stable conditions. Hanna (1969), following a suggestion of Laikhtman (1961), has shown that the observed depth D of the boundary layer can be described in terms of the velocity U_g at its top and the (potential) density gradient through it by

$$D = 0.75 U_g \Big/ \left(\frac{g}{\rho}\frac{\Delta\rho}{\Delta z}\right)^{\frac{1}{2}}. \qquad (9.2.11)$$

This is equivalent to the statement that the overall Richardson number of all deep stable atmospheric boundary layers adjusts itself to a value of $\frac{1}{2}$ (cf. §§ 5.3.2 and 10.2.1). It is not as practically useful as (9.2.4) (since it involves a derived density gradient which is not easily observed), but (9.2.4) and (9.2.11) can be regarded as alternative 'flux' and 'gradient' forms resulting from related physical arguments.

9.2.4. *Other factors limiting the depth of a mixed layer*

So long as the turbulence near an interface is maintained in some way, the inviscid entrainment processes described above would continue to cause a well-mixed surface layer to deepen indefinitely. One way of counteracting this tendency and producing a steady state has been mentioned – large scale upwelling (in the ocean) or subsidence (in the atmosphere), with an associated divergent flow in the layer itself. For these geophysical flows, however, a steady state also becomes possible because of two factors not yet considered. It would be wrong to leave the impression that a simple entrainment model is always the relevant one to apply, so a few qualitative remarks should be made about each of these processes.

For the first time in this book, we must introduce explicitly the effect of the earth's rotation. In a rotating system, the influence of a boundary stress does not penetrate indefinitely, but is limited to the Ekman layer, in which it is entirely balanced by the Coriolis forces. (See, for example, Phillips (1966*a*, p. 228) for a fuller discussion.) Both the direction and magnitude of the mean velocity vary with depth, in a manner which depends in detail on the mixing, but in a rotating fluid of constant density (5.1.1) can be replaced by

$$\frac{\mathrm{d}\mathbf{u}}{\mathrm{d}z} = \frac{u_*}{z}\,\mathbf{h}\left(\frac{fz}{u_*}\right), \tag{9.2.12}$$

where f is the component of angular velocity about a vertical axis, u_* is the friction velocity, and $\mathbf{h}$ is some function of the non-dimensional parameter in brackets. In the rotating case, therefore, with a boundary stress but negligible buoyancy flux, the lengthscale $L_\mathrm{e} = u_*/f$ ('the depth of the Ekman layer') becomes relevant instead of the Monin–Obukov length L_b defined in (5.1.8) and implied by (9.2.4).

There is some confusion of these lengthscales, especially in the oceanographic literature where the 'upper mixed layer depth' and 'Ekman layer depth' often seem to be regarded as synonymous. This identification is valid only when $L_\mathrm{b} \gg L_\mathrm{e}$. Then the forced convection region (in the absence of rotation) would include the whole of the Ekman layer, and so rotation determines the extent to which the surface effects can penetrate. The opposite case, where

$L_b < L_e$, is the one already considered in arriving at (9.2.4). The penetration of a wind-stirred layer is then limited by buoyancy, before rotation can have an appreciable effect on the momentum flux.

The second factor which should be mentioned is the effect of a stable density gradient outside a well-mixed layer. Under these conditions momentum and energy can be lost from the layer (and therefore become unavailable for local mixing) in another way. They can be radiated away in the form of internal gravity waves, and the most favourable circumstances for this to happen can be found by examining the relations given in §2.2.2. If the forcing frequency ω is too high, waves cannot be generated, and no energy is radiated at all. When $\omega < N$, wave propagation is possible, and Townsend (1965, 1966) has shown that both convective and shear generated turbulence in the atmospheric boundary layer can produce disturbances of the interface which permit radiation. In the latter case most of the wave energy is in components having a phase velocity close to the convection velocity V of the dominant disturbances in the boundary layer, i.e. those which satisfy a 'resonance' condition, and these have a wavelength near $L_1 = 2\pi VN^{-1}$, where N is the buoyancy frequency of the region above the interface (not of the much more stable interface itself). Inserting appropriate numerical values for the atmospheric boundary layer, Townsend showed that wave amplitudes of order 100 m could develop in a few hours.

Detailed calculations for more general environmental conditions (including a shear outside the boundary layer) led Townsend (1968) to conclude that the rate of radiative energy loss from the boundary layer in both the atmosphere and the ocean can be large enough to affect the motion of the layer itself. He showed that the fraction of the energy produced in the outer part of the layer which is radiated away in gravity waves is a strong function of the ratio L_0/L_1, where L_0 is the scale of the turbulence (comparable with the boundary layer thickness), and L_1 has been defined above. The radiated energy is negligible if L_0 is small compared with V/N, but if $L_0 \sim V/N$, the thickness of the turbulent layer is near the upper limit set by the removal of energy in gravity waves. (Compare with (9.2.11).) The numerical values estimated for the atmosphere

and ocean are such that the limits set by this wave radiation process and by the earth's rotation are approximately equal in each case.

Wave energy supplied to the interior in this (and other) ways also plays an important part in the transport and mixing processes outside the boundary layer. These will form the subject of chapter 10.